REVISTA MEXICANA DE CIENCIAS GEOLÓGICAS

Revista Mexicana de Ciencias Geológicas, v. 42, núm. 1, abril 2025, p. 1–16
ISSN-L 2007-2902
https://rmcg.unam.mx

Type: Original Research

OPEN ACCESS

Experimental study of infiltration through subsidence-reactivated surface discontinuities

Martín Hernández-Marín[1,3], Norma González-Cervantes[1], Lilia Guerrero-Martinez[1], Christian Emmanuel Rodríguez-Padilla[2], and Jesús Pacheco-Martínez[1,3]

[1] Departamento de Ingeniería Civil, Universidad Autónoma de Aguascalientes, Av. Universidad No. 940, Ciudad Universitaria, C.P. 20100, Aguascalientes, Mexico.
[2] Maestría en Ingeniería Civil, Universidad Autónoma de Aguascalientes. Av. Universidad No. 940, Ciudad Universitaria, C.P. 20100. Currently working at Geofísica Aplicada a la Geotecnia S.C., Mexico.
[3] Observatorio de Riesgos Hidrogeológicos, Universidad Autónoma de Aguascalientes, Av. Universidad No. 940, Ciudad Universitaria, C.P. 20100, Aguascalientes, Mexico.
** Corresponding author (M. Henández-Marín): martin.hernandez@edu.uaa.mx*

Editors:
Natalia Pardo Villaveces
Eric Morales Casique

How to cite:
Hernández-Marín, M., González-Cervantes, N., Guerrero-Martinez, L., Rodríguez-Padilla, C.E., & Pacheco-Martínez, J. (2025). Experimental study of infiltration through subsidence-reactivated surface discontinuities. *Revista Mexicana de Ciencias Geológicas*, *42*(1), 1–16. DOI: http://dx.doi.org/10.22201/igc.20072902e.2025.1.1836

Manuscript received: July 13, 2024
Corrected manuscript received: January 23, 2025
Manuscript accepted: January 23, 2025
Published Online: April 1, 2025

ABSTRACT

The main objective of this work is to investigate the influence of surface geological discontinuities on the hydraulic properties of the subsoil, studying an area affected by a fault (surface scarp) and a fracture (horizontal surface opening), which are separated by about 18 meters each other, forming part of a discontinuity system located within the Aguascalientes Valley (VA), Mexico. Both discontinuities are currently active due to the process of subsidence that the VA has been experiencing for more than 45 years, this emphasizes the relevance of this study since in most cases the studies are focused on regional inactive faults. In addition, studying some of the hydraulic properties of active discontinuities in the VA is significant because this valley currently has a large number of such structures with similar geologic conditions. As part of the methodology, 33-meter profiles of infiltration rates and hydraulic conductivity were obtained by applying permeability tests in the field, as well as 38-meter Electrical Resistance Tomography (ERT) profiles, in order to obtain and analyze the general characteristics of the subsoil and discontinuities. Subsequently, four ERT tests were applied in synchrony with punctual permeability test. The first ones in profiles of 14–17 meters, and the second ones in four points located at distances of under one meter from the discontinuities. These synchronized tests made it possible to visualize, in ERT profiles, the flow path of water injected into the subsurface through the permeameter, as well as the influence of the discontinuities on the hydraulic parameters mentioned above. The results show that the hydraulic parameters obtained in the areas close to the discontinuities, particularly the fault, are higher than those in the areas more distant from both discontinuities, probably due to their constant mechanical activity, being these increases of up to two orders of magnitude, obtaining maximum values of 2.08E-03 m/s for the infiltration velocity and 5.22E-05 m/s of hydraulic conductivity. On the other hand, observations from the simultaneous ERT-permeability tests suggest that discontinuities, particularly the fault, directly influence the path of infiltrated water, allowing the water to tend to move towards the displacement plane.

Keywords: hydrogeology; Aguascalientes Valley; subsidence-activated discontinuities; field permeameter; Electrical Resistance Tomography (ERT); infiltration dynamics.

RESUMEN

El presente trabajo tiene como objetivo primordial el investigar la influencia de las discontinuidades geológicas superficiales sobre las propiedades hidráulicas del subsuelo, estudiando un área afectada por una falla (escarpe superficial) y una fractura (abertura horizontal superficial),

las cuales se encuentran separadas por aproximadamente 18 metros entre sí, formando parte de un sistema de discontinuidades localizado dentro del Valle de Aguascalientes (VA), México. Ambas discontinuidades están actualmente activas debido al proceso de subsidencia que ha estado experimentando el VA desde hace más de 45 años, lo que enfatiza la relevancia de este estudio ya que, en la mayoría de los casos, los estudios se enfocan sobre fallas regionales inactivas. Además, el estudiar algunas propiedades hidráulicas de las discontinuidades activas del VA es significante ya que este valle actualmente cuenta con una gran cantidad de estas estructuras con condiciones geológicas similares. Como parte de la metodología, se obtuvieron perfiles de 33 metros de tasas de infiltración y conductividad hidráulica aplicando pruebas de permeabilidad en campo, así como perfiles de Tomografía Eléctrica Resistiva (TER) de 38 metros, con el fin de determinar y analizar las características generales del subsuelo y discontinuidades. Posteriormente, se aplicaron cuatro ensayos TER en sincronía con pruebas puntuales de permeabilidad, los primeros en perfiles de 14–17 metros, y los segundos en cuatro puntos situados a distancias inferiores a un metro de las discontinuidades. Estos ensayos sincronizados permitieron visualizar, en perfiles TER, el recorrido del flujo de agua inyectada en el subsuelo a través del permeámetro, así como la influencia de las discontinuidades sobre los parámetros hidráulicos mencionados. Los resultados muestran que los parámetros hidráulicos obtenidos en las zonas próximas a las discontinuidades, en particular de la falla, son mayores que en las zonas más distantes a ambas discontinuidades, debido probablemente a la su constante actividad mecánica, siendo estos incrementos de hasta dos órdenes de magnitud, obteniéndose valores máximos de 2.08E-03 m/s para la velocidad de infiltración y 5.22E-05 m/s de conductividad hidráulica. Por otro lado, las observaciones realizadas a partir de los ensayos simultáneos TER-permeabilidad sugieren que las discontinuidades, en particular la falla, influyen directamente en la trayectoria del agua infiltrada, permitiendo que el agua tienda a dirigirse hacia el plano de desplazamiento.

Palabras clave: *hidrogeología; Valle de Aguascalientes; discontinuidades activadas por hundimiento; permeámetro de campo; Tomografía de Resistencia Eléctrica (ERT); dinámica de infiltración.*

INTRODUCCIÓN

Surface discontinuities, whether faults (surface scarps), or fractures (horizontal surface openings), are of continuous technical and scientific interest in hydrogeology because of their complex hydraulic behaviors, for example during groundwater pumping (António and Pacheco, 2002; Ochoa-González *et al*., 2015) and in the dynamics of local or regional groundwater flow (Ball *et al*., 2010; Bense and Person, 2006; Caine and Tomusiak, 2003; Cilona *et al*., 2015; Fronzi, *et al*., 2021). More examples of the influence of these structures on hydrogeological processes include cases of hydraulic communication between aquifers and surface water. For example, Martin *et al*., (2023) and Reyes-Cedeño *et al*., (2023), relied on geophysical techniques and level data from pumping and monitoring wells to achieve their objectives, or in the case of Stoessell and Prochaska, (2005), who used geochemical data to evidence the upward migration of deep fluids through a regional fault. One of the reasons for this complex response is that discontinuities can behave as a channel or a barrier to horizontal groundwater flow (Bense *et al*., 2008; Bense and Person, 2006; Bredehoeft *et al*., 1992).

The preferential groundwater flux across discontinuities is conditioned not only spatially but also temporally (Bense *et al*., 2013; Constantin *et al*., 2004). For example, Hernández-Marín *et al*., (2017) observed that the Oriente fault in the VA can restrict the horizontal flow, but favor the vertical, at least in the studied section, causing this structure to behave as a path of infiltration and thus, encouraging aquifer recharge. On the other hand, a discontinuity usually represents the preferential flow at some period in its geological history, leaving in several cases, traces of its frequent transit through its zone of influence, as shown in Figure 1, where a reddish coloration is observed, which is probably caused by the oxidation process of some minerals during the flow of water. In this regard, the different local and regional dynamics in the zone influenced by a discontinuity can contribute to produce conditions for periods of non-flow and others of flow (Constantin *et al*., 2004). In fact, several studies have tried to explain the role of discontinuities at local and regional levels with variable results (Bense *et al*., 2003; Fronzi, *et al*., 2021; Helena *et al*., 2016; Petrie *et al*., 2014; Seaton and Burbey, 2005).

The activity *vs.* inactivity of discontinuities, is also a comparation that can be considered crucial when their hydraulic properties are evaluated, for example, for an inactive discontinuity, one of the most important intrinsic variables could be the remained structural architecture, which can include deformation bands, secondary displacement planes, zones of cataclysm and granulation (Antonellini and Aydin, 1994; Bense and Person, 2006; Heynekamp *et al*., 1999). On the other hand, for an active discontinuity, whether reactivated or recently formed, along with some of the factors mentioned above, other factors could be the direction and magnitude of the stresses that affect it (Balsamo and Storti, 2010; Caine *et al*., 1996; Hernández-Marín *et al*., 2017), as well as to the mechanical resistance of the materials adjacent to the discontinuity, including its mechanical zone of influence. For example, in an active discontinuity affected by tensile stress, as is the case of normal faults, some characteristics such as infiltration capacity could be more favored than those in which compressive stress predominate (Hernandez-Marín *et al*., 2017). In the same way, the stresses that exceed the resistance of the materials of the fault zone could increase the secondary porosity in the form of small cracks, which in turn would increase their permeability and infiltration capacity.

On the other hand, advances in the application of geophysical methods have permitted to visualize the path of liquids through a soil affected by a discontinuity. For example, Rugh and Burbey (2008)

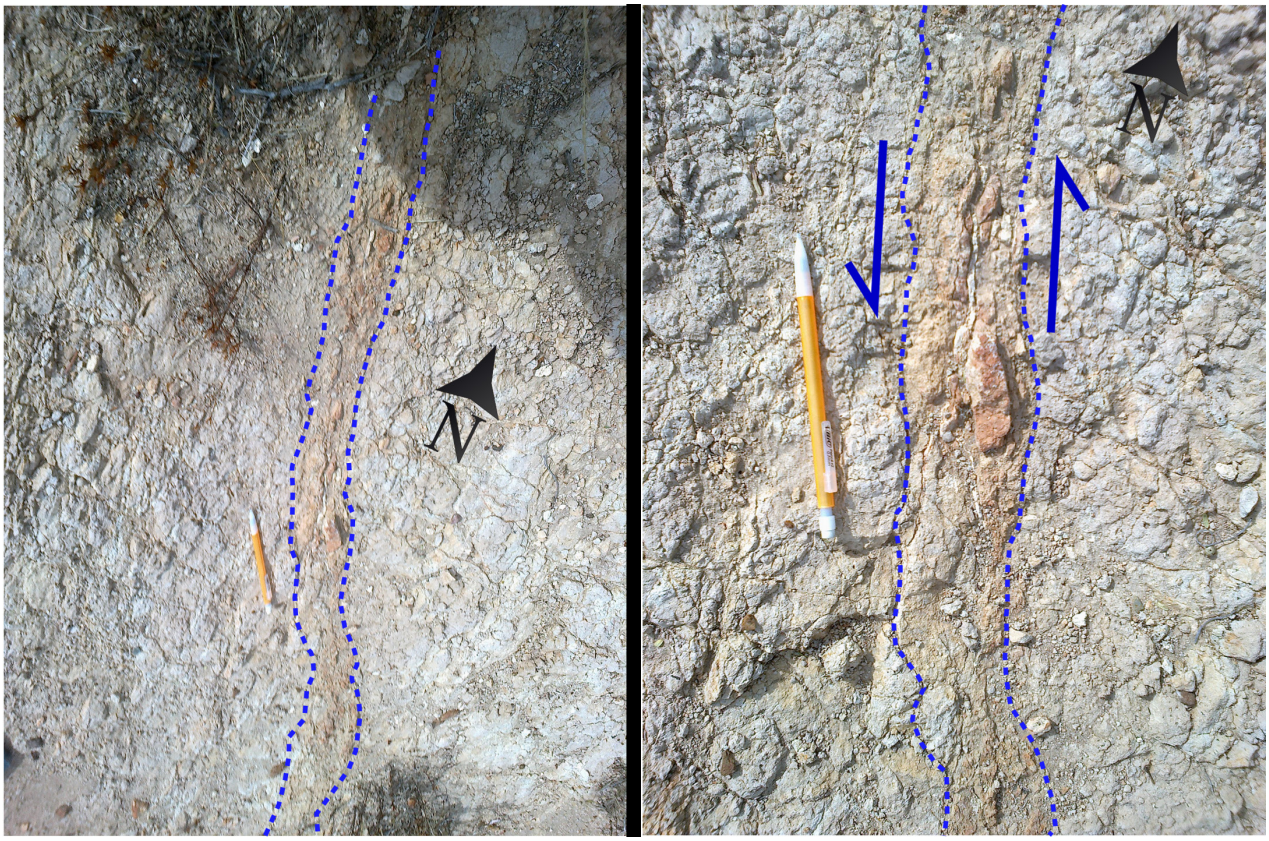

Figure 1. Plan view of an active discontinuity zone with lateral displacements in the Aguascalientes Valley, Mexico. The reddish coloration in the fault zone could be attributed to the preferential passage of water that would cause the oxidation of some minerals contained in the soil.

used the electrical resistivity technique, complementing other chemical and physical tests to define the preferential route of groundwater flow from a surface water source. They found that the path of water in the subsurface is strongly influenced by a series of fractures in the rock. Gannon *et al*., (2012) included in their study a series of measurements with electrical resistivity using the dipole-dipole technique to determine whether an inactive regional fault would behave as a barrier or flow. They found that the portion of the fault under study has a very low permeability, similar to that of the casing rock (limestone).

It is important to clarify that water infiltrating through a discontinuity does not necessarily represent aquifer recharge, because this water may not reach the water table. However, if the discontinuity deepens to or near to it, and this discontinuity permits vertical infiltration, then it can be considered as a recharge channel. This is relevant for the VA because it is believed that the ancient faults that originated the VA (Oriente and Poniente faults) may deepen until the local aquifer.

The main objective of this work is to apply a methodology to two surface discontinuities, in order to obtain some of their hydraulic parameters such as infiltration rate and hydraulic conductivity, providing elements to understand the hydraulic response of a discontinuity system (fault-fracture) that has been reactivated by a process such as subsidence, and therefore is currently active. The study includes the main area of activity, which is usually the fault plane, as well as the adjacent material that could be mechanically affected by the dynamics of the discontinuities, this is the so-called fault zone. The discontinuity system evaluated consists of two active local discontinuities, a normal fault and a fracture, both acting on a sequence of unconsolidated material in the Aguascalientes Valley.

CHARACTERISTICS OF THE STUDY AREA

The study area is located into the Aguascalientes Valley (VA), in the central region of Mexico. This zone is geologically inside the Aguascalientes Graben (AG), and physiographically located within the Central Mesa and bordering the Sierra Madre Occidental (Figure 2). Despite the AG presented an initial stage of geological activity in the Oligocene (Nieto-Samaniego *et al*., 2005, Loza-Aguirre *et al*., 2008, González-Cervantes *et al*., 2019), it has been currently recognized that this graben has little or no tectonic and magmatic activity, as indicated by its level of erosion (Nieto-Samaniego *et al*., 2023). In addition, the extensional structural activity that occurred in the AG had an east-west direction, thus, this graben is currently delimited by two main normal faults flanking the valley with a preferential N-S direction (Nieto-Samaniego *et al*., 2023). These two faults are locally named Oriente fault, with a westward dip, and Poniente fault, with an eastward dip.

The activity of the last 50 years that have experienced most discontinuities in the VA, including the reactivation of pre-existing ones, is closely related to the subsidence process (Aranda-Gómez, 1989; Pacheco-Martínez *et al*., 2013; Hernández-Marín *et al*., 2015). In fact, the activity of discontinuities in the VA is particularly critical when land subsidence occurs differentially. The first reports suggest discontinuities commenced to appear in the late 1970s (Aranda-Gómez, 1989). Recent surface discontinuities in the VA are mostly observed almost parallel to the two main normal faults, among which there are several normal faults some with oblique movement.

The extraction of groundwater is a key process that has triggered the occurrence of subsidence and surface discontinuities in the VA,

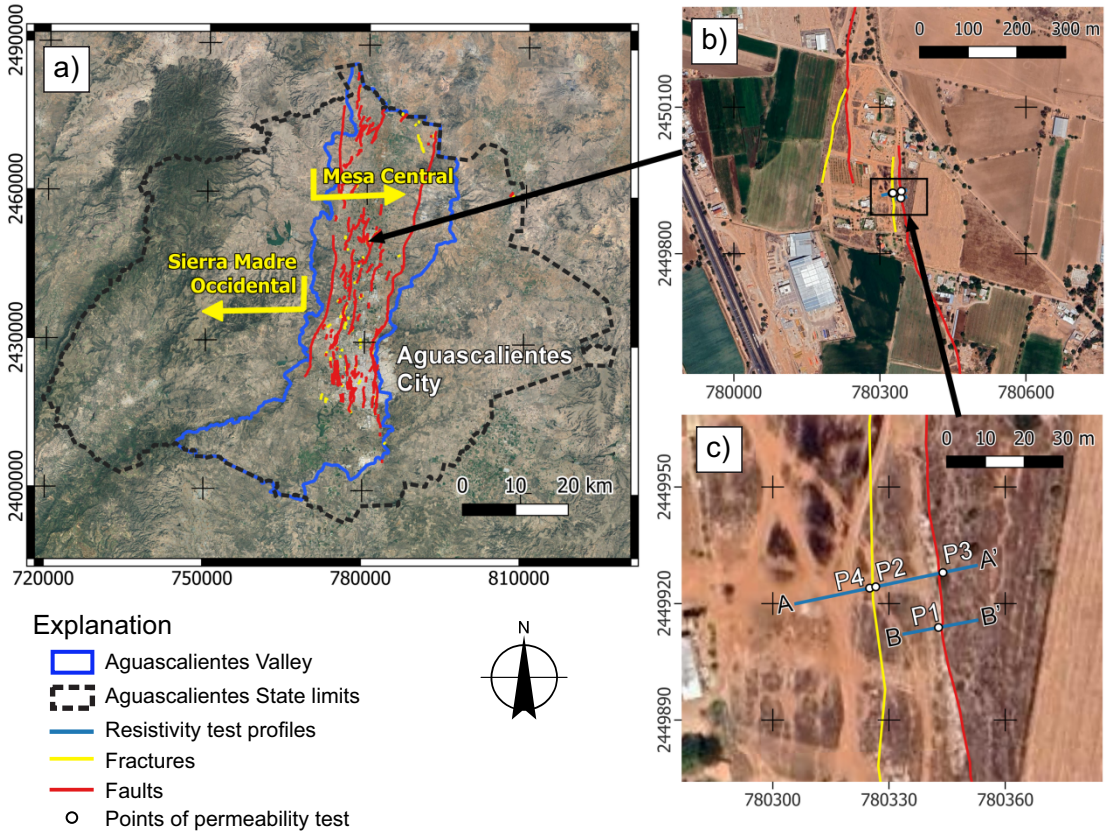

Figure 2. Study area at different scales. a) General view at the state and valley scale, including the relative position of the two main physiographic provinces. b) View of the study area at the community and urban scale. c) Close-up view of the experimental area. Points P1 to P4 indicate the location of the permeability tests. The blue lines A-A' and B-B' show where the ERT profiles were made. The general ERT profile and the permeability profile were made in line A-A', the latter by applying these tests at different points on this line.

being a direct consequence of the increase in the need for water to satisfy current demands. The descent of the local water table due to groundwater pumping is critical nowadays, since by 2018 the water table reached a maximum depth of 90 m in some regions (Hernández-Marín *et al*, 2018). Unfortunately, there are not published documents with more recent data related to water table depth, but we believe that it has reached more than 200 m in some points, according to the information provided by some local farmers. According to the state government, it is estimated that the current annual volume of groundwater recharge in the local aquifer is around 250 Mm^3, while the discharge (induced and natural) is close to 350 Mm^3 (Aguascalientes, Gobierno del Estado, 2022), resulting in an annual deficit close to 100 Mm^3. Other characteristic of this valley regarding the availability of water, is that its climate is semi-arid with low precipitation (~500 mm/yr) and high evapotranspiration (~2000 mm/yr), and that most of the human settlements of the state of Aguascalientes are located on the VA, including the capital city, which makes more critical the need for water in this valley.

Descent of groundwater levels along with the accumulation of surface constructions, have caused the increase of effective stress in subsoils, this instead has caused the reactivation of pre-existing discontinuities buried in the VA. This process has been verified through observations in trenches and quarries, as well as by interpretations in the results of geophysical methods (Pacheco-Martínez *et al*., 2013; Hernández-Marín *et al*., 2015). In many cases, the discontinuities are observed arranged in groups of two or more individual structures as a result of the intense accumulation of stress in the vicinity of an initially isolated discontinuity, as a mechanical response of the soil to the imposed stress, thus for example, several fractures of the VA are presented as branches of the main faults (Lee *et al*., 1993).

On the other hand, the deposits that fill the valley and that are being affected by these discontinuities are mainly of fluvial and alluvial origin (Aranda-Gómez, 1989; Servicio Geológic o Mexicano, 1998; González-Cervantes *et al*., 2019). According to observations in several quarries and other open pits within the valley, the local soil contains mainly gravel and sand, with minor proportions of silts and clays. In addition, the soil can be observed with different degrees of diagenetic alteration (variation in lithification), likewise, epiclastic and volcanic (mainly ignimbrite and tuff) deposits have been recognized within the valley, with lesser amounts of calcareous sediments, opaque chalcedony concretions and selective replacement. To complete the description, the remarkable presence of caliche has been observed in several points of the valley, which is observed as a calcium carbonate cement or as carbonate horizons in the subsoil (Gaytan-Molina, 2021).

The specific study of this research was developed in the central part of the VA, in the municipality of Pabellon de Arteaga. This area was chosen due to three main reasons: 1) due to the permits granted by the owners for its realization, 2) because there was sufficient space for the management and implementation of the instrumentation, and 3) by the accessibility of the place so that the entrance of vehicles carrying the equipment was granted. The chosen study area was significant because it includes two adjacent discontinuities, a normal fault and a fracture, officially named by the state government as "subestación 2 fault"

and "subestación 2 fracture", according to the information consulted in the Geological Faults and Cracks Information System (SIFAGG) https://www.aguascalientes.gob.mx/sop/sifagg/web/mapa.asp (Figure 2). According to this website, the length of the fault of this study is 495.98 m and is observed in the field as a structure with a surface vertical offset of up to 70 cm, a maximum opening of about 60 cm, a strike angle of 340° and a dip angle close to 86° toward the west. The sedimentary material observed in this fault is clayey silt with an upper layer of caliche with some rusty cemented soil. While the length of the fracture is 150.26 m and is located about 18 meters westward of the fault, with a maximum opening of about 30 cm, and strike angle of 355°, is observed in a segment close to 10 m long as a fault since it presents a vertical differential displacement of about 30 cm, with a dip angle of 89° toward the east, therefore forming a small graben with the fault. As mentioned above, this fault-fracture structural system is very common in the VA.

METHODOLOGY

In general, the methodology consisted of applying Electrical Resistance Tomography (ERT) and subsurface permeability techniques in the experiment area (Figures 2 and 3). The first basically involved applying an electrical current to subsoil through surface electrodes and analyzing the soil response. Under this technique, the less moisture and salinity in pore water in the soil the more resistive the soil. While the permeability test consisted of measuring the hydraulic conductivity and infiltration rate parameters of the soil. Both techniques were initially applied in a line on the surface approximately perpendicular to the planes of both discontinuities (line A-A', Figure 2c), obtaining general profiles of ERT (38 m) and permeability (33 m). These general profiles were performed to observe the overall behavior of both discontinuities to the application of the two techniques. Subsequently, 14 to 17 meters long ERT tests were applied partly in line A-A' and completely in line B-B' (Figure 2). These tests were applied concurrently with permeameter test at four selected points adjacent to both discontinuities, two in each one, as they are observed in Figure 2 (points P1 through P4). During these permeability tests on each of these four points, water was constantly infiltrated as the ERT test was performed. The main idea of this practice was to obtain the variations of electrical resistivity/conductivity of the subsoil as the water was infiltrated through the upper soil layers. This was relevant since the path of the groundwater flow was captured.

All ERT tests in this research were performed using the "dipole-dipole" arrangement, as it is one of the most recommended to capture moisture in the soil (Gannon *et al.*, 2012), while the equipment used was a resistivity meter SYSCAL Jr. In Figure 4, part of the electrode arrangement can be observed when applying the ERT technique. Once the ERT profiles were completed, the returned data were analyzed and processed in the computer program ResIPy v. 3.4.5.

Application of general Electrical Resistance Tomography (ERT) profiles

Usually, for the application of the ERT test, several electrodes partially embedded in the ground and electrically connected to each other and to the power source by a suitable cable are used. This method was used in this research because it is one of the most effective for detecting high and low moisture zones of the soil (Seaton and Burbey, 2005). That is, the zones of high moisture correspond to the zones of low electrical resistivity and *vice versa*. For the stage to obtain the general ERT profile, 20 electrodes were used with a separation between them of two meters. Also, they were arranged in a line perpendicular to the plane of the discontinuities under study (Figure 3), obtaining a two-dimensional profile on the soil resistivities with a prospecting depth close to eight meters.

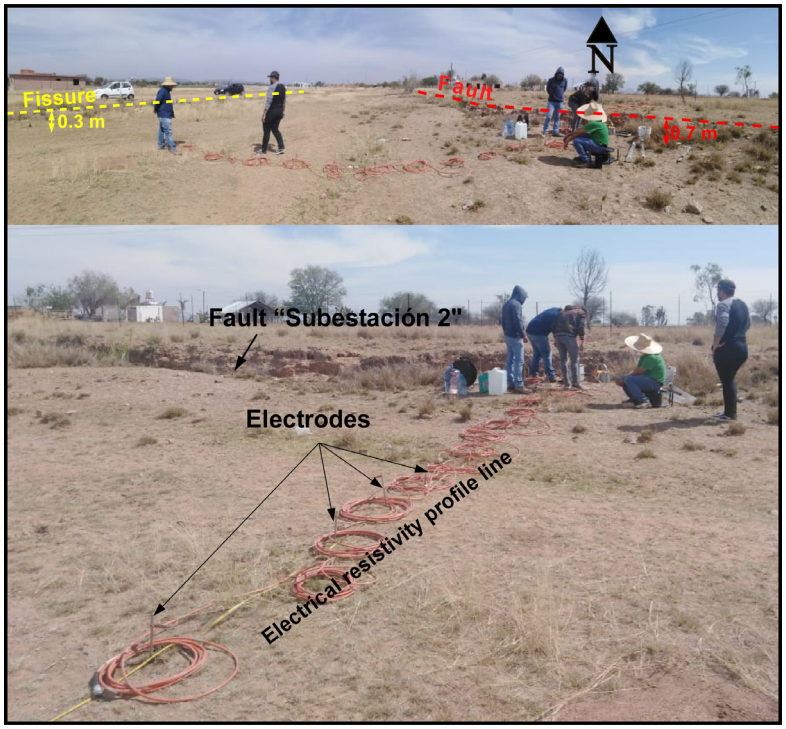

Figure 3. Photograph during fieldwork where both discontinuities are shown. The photographs were taken during the application of the ERT method.

Measurement of soil permeability

To obtain the infiltration capacity and hydraulic conductivity of the upper part of the soil affected by discontinuities, a Pask permeameter was used (Figure 4). Thus, the parameter known as saturated hydraulic conductivity in the field (K_{fs}) was obtained using the constant-head technique (Elrick and Reynolds, 1986; Reynolds, 1993). This parameter is usually less or equal to that of a previously saturated soil (Reynolds, 1993), this is due to the hydraulic barrier that gas bubbles trapped in the soil can cause (Constantz *et al*., 1988). Despite that, K_{fs} is usually used for design conditions in infrastructure studies since it represents the conductivity of the soil under realistic conditions.

In general, to obtain the hydraulic parameters in the field, the Pask permeameter must be filled with water and placed into a hole in the soil, which has been previously free of vegetal material. This hole must have a diameter slightly larger than that of the infiltration tube, (lower tube shown in Figure 4), so that such tube can be embedded. In addition, the hole must have an adequate depth so that the permeameter can maintain static in a vertical position during the filtering of water and data collection, also allowing the perforation zone located at the bottom in the infiltration tube to be totally submerged in the water contained in the hole during the filtering process. It is important to mention that the height of the water in the soil hole is kept constant during the test since the water that infiltrates into the soil is quickly replaced by the water from the permeameter. This process is essential in the test since the volume of water that the permeameter transfers can be quantified and permits the equations to be applied and then to obtain the desired hydraulic parameters.

The primary data obtained during the field test are the variation of the water level in the permeameter reservoir tube (upper tube shown in Figure 4), and the elapsed time, because once the permeameter is embedded in the hole, the water begins to infiltrate into the subsoil at a flow rate that mainly depends on its hydraulic conductivity. At the beginning of the test, the infiltration rate is usually variable but becomes constant after a few minutes. At this time, the following expression can be applied (Reynolds, 1993):

$$K_{fs} = \frac{CQ}{\left[2\pi H^2 + C\pi a^2 + \left(\frac{2\pi H}{\alpha^*}\right)\right]} \quad (1)$$

In which a is the radius of the hole in the ground (cm), which is 5.5 cm for this study; α^* is a parameter related to the structure of the soil, which depends on the grain size and arrangement of the grains, resulting generally in high permeability for well-structured soils. This parameter can be obtained from Table 1 (cm^{-1}) (Reynolds, 1993) and for this study, a value of 0.36 was considered; H is the hydraulic head of the hole in the ground in which the permeameter is embedded, considering a value of 13 cm for this device (Dynamic Monitors, 2022); Q is the infiltration flow rate ($cm^3 min^{-1}$) and can be obtained by multiplying the rate of variation of water height in the reservoir tube (cm/min), by the section of that tube, which is equal to 53.46 cm^2 for this type of device (Dynamic Monitors, 2022). Finally, C is a dimensionless shape factor that is obtained from the graph of Figure 5 (Elrick and Reynolds, 1986), which for this study was equal to 1.01, considering that the curve that best adapted to the type of soil of the field is the number 1, while the value of H/a was around 2.36. It should be noted that the total volume that the permeameter can transfer to the soil for each test is as much as 4000 cm^3.

The results of this permeability technique should be corrected according to the temperature of the water used in the experiment, for this the following equation must be used (Streeter and Wylie, 1975):

$$Ka = K_{fs}\, C\mu_k / \mu_a \quad (2)$$

Where Ka is the corrected hydraulic conductivity; μ_k is the viscosity of the water used in the permeameter; μ_a is the viscosity of the water at the operating temperature, related to the design of the device. For this work, water with an ambient temperature of 18 °C was used, then, according to the permeameter user guide (Dynamic Monitors, 2022), the μ_k/μ_a ratio is equal to 0.762, this indicates that the final equation to obtain the corrected hydraulic conductivity is:

$$Ka = 0.762\, K_{fs} \quad (3)$$

For this investigation, 33 tests with the permeameter were carried out, separated on the surface by one meter each other and in a profile line perpendicular to the two discontinuities as shown in the diagram of Figure 6.

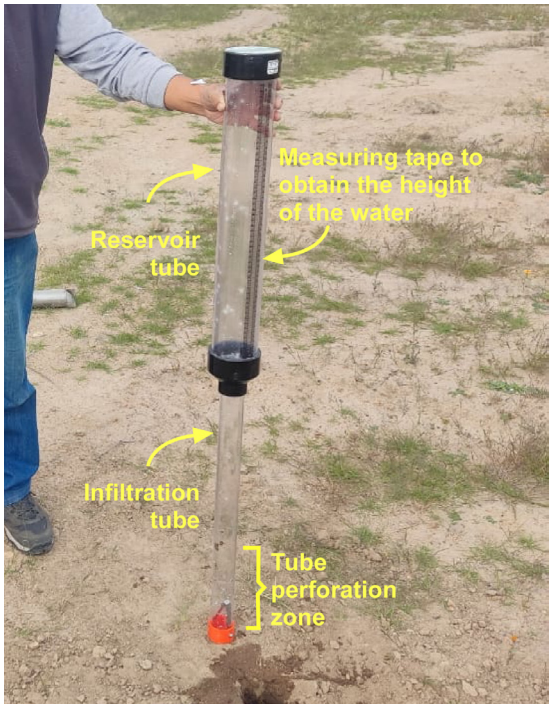

Figure 4. Photograph of the Pask permeameter used in the experiments, pointing out some of its main components. The perforation zone indicated in the image contains several holes around the tube and its function is to transfer the water to the hole in the soil.

Table 1. Values for the α^* parameter according to the structure and texture of the soil, taken from the Pask permeameter manual (Dynamic Monitors, 2022).

α^* (cm^{-1})	Soil structure and texture
0.36	Coarse sands and gravelly sands, highly structured soils with large cracks and/or macropores.
0.12	Most structured soils and medium textures material sands, also includes structured clays and loamy soils, and unstructured medium single-grain sands. Generally, this category is the most common for most soils.
0.04	Porous, fine-textured, and massive soils, also unstructured fine soils and very fine to fine structureless sands.
0.01	Compacted, unstructured clayey soils, for example, landfills caps and liners, also lacustrine or marine soils.

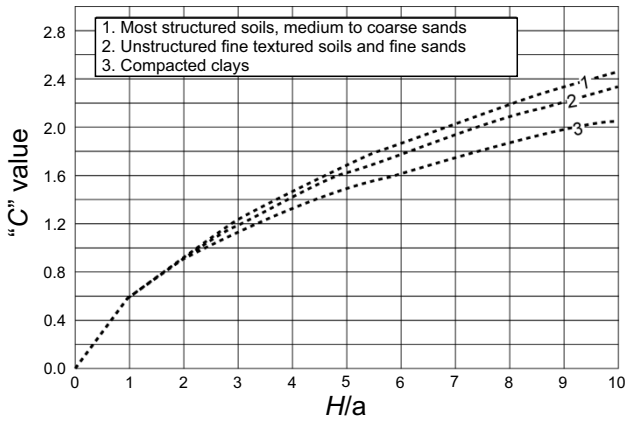

Figure 5. Graph to obtain the values of the parameter ***C*** as a function of the parameters *H* and a, according to (Reynolds, 1993). Each curve corresponds to a type of soil as explained in the figure.

Application of simultaneous electrical resistivity and permeability tests

As mentioned above, several ERT tests were applied at four infiltration points concurrent to permeability tests, two points near the fracture (P4 and P2) and two near the fault (P1 and P3; Figure 2c). In total, five subsoil resistivity measurements were completed for each of the four selected points, one before the infiltration process and the remaining four were simultaneous to the infiltration of water. These ERT tests permitted to obtain profiles of resistivity with a prospecting depth close to 3.5 m and almost 14 – 17 meters long, with 20 electrodes placed at every 0.7 – 0.85 meters on the surface.

To better observe the flow of water in the soil after the ERT tests, a small amount of comestible salt (NaCl) was added to the infiltrating water, a practice that has worked in other similar cases without affecting the environment, for example, in the research of Rugh and Burbey (2008), who used KCl and KBr. In this case, approximately 20 grams of salt were added for every liter of water, obtaining brackish water. It should be mentioned that these ERT tests lasted approximately 80 minutes and that during this time water was being added to subsoil with the permeameter.

RESULTS

In general terms, the results obtained show that both parameters, the infiltration rate and hydraulic conductivity, increased in the soil adjacent to both discontinuities. Additionally, the plane of displacement of the discontinuities, in particular the fault, is presented as a preferential vertical flow channel, at least in the first meters of depth.

General profile of infiltration and hydraulic conductivity

The 33 permeability tests in the general profile (A-A') performed with the Pask permeameter allowed to obtain varied data on both infiltration rate and hydraulic conductivity, as shown in Table 2. For the first parameter, the results yielded values of a maximum of 12.5 cm/min (2.08E-03 m/s), which was obtained at a distance under two meters from the fault plane, while the smallest measurement obtained was 0.1 cm/min (1.67E-05 m/s). The average infiltration rate for the overall profile was 2.68 cm/min (4.46E-04 m/s), although the geometric mean was 1.55 cm/min (2.58E-04 m/s). On the other hand, the hydraulic conductivity (*Ka*) data varied by two orders of magnitude along the profile ranging from a maximum of 5.99E-05 m/s to a minimum of 4.79E-07 m/s, with a geometric mean of 7.42E-06 m/s and an average of 1.28E-05 m/s. The significant differences in the data for each parameter are indicative of the hydraulic differences between the unaffected soil and the soil affected by the discontinuities. There may be implicit errors associated with the measurements, but we believe that these potential errors do not significantly affect the final results.

Figure 7 shows the profile A-A' (see Figure 2c) with the results of the permeability tests. It should be noted that the two points with the highest values of both parameters are located near the fault and in general, the higher values are mainly presented between the fault and the fracture. As observed, the values of both parameters are lower by several orders of magnitude to the west of the fracture and at the east of the fault, except for a single point with high values at 8.5 meters to the east of the fault. In the area between both discontinuities, several small surface cracks (openings less than 5 mm) were observed, likely influencing the values of the hydraulic parameters. These small cracks are probably related to the mechanical activity of both discontinuities and form a network of subsurface cracks, although further investigation is required to confirm this.

Electrical resistivity profiles under initial conditions

As mentioned above, a general ERT profile was applied to characterize the study area and to better understand the initial conditions of the local subsoil in response to an electric current (line A-A'). As can be seen in Figure 8, the resulting profile suggests that both discontinuities have almost vertical displacement. The areas of low resistivity, lower than 25 Ω·m, could be related to a number of features, such as the presence of clay, high compaction, etc. They could also be related to high moisture retained by the soil, for example, the one closest to the fault plane, which is observed to a depth of two meters. The areas with high resistivity, more than 300 Ω·m, are observed closer to the surface and could be associated with air, for example in the location of the fault. These areas of high resistivity could also be associated with compacted soil due to the presence of dirt roads and pedestrian paths.

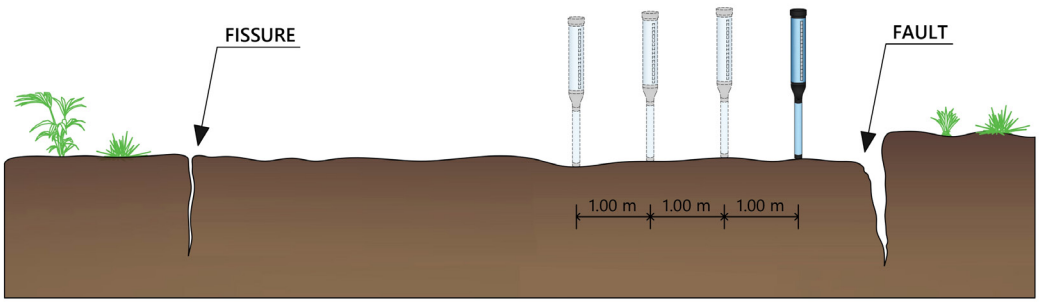

Figure 6. Scheme of the application of the Pask type permeameter to determine the infiltration rate and the saturated hydraulic conductivity of K_{fs}. The diagram shows how the tests with the permeameter were applied at different points in a surface line.

Table 2. Data derived from the field permeability test.

Point	Infiltration rate		Q		K_{fs}	K_a	
	cm/min	m/s	cm^3/min	cm^3/s	cm/s	cm/s	m/s
1	0.70	1.17E-04	37.42	0.62	4.40E-04	3.35E-04	3.35E-06
2	0.60	1.00E-04	32.08	0.53	3.77E-04	2.87E-04	2.87E-06
3	1.50	2.50E-04	80.19	1.34	9.43E-04	7.19E-04	7.19E-06
4	0.90	1.50E-04	48.11	0.80	5.66E-04	4.31E-04	4.31E-06
5	1.00	1.67E-04	53.46	0.89	6.29E-04	4.79E-04	4.79E-06
6	0.60	1.00E-04	32.08	0.53	3.77E-04	2.87E-04	2.87E-06
7	0.40	6.67E-05	21.38	0.36	2.51E-04	1.92E-04	1.92E-06
8	1.00	1.67E-04	53.46	0.89	6.29E-04	4.79E-04	4.79E-06
9	0.40	6.67E-05	21.38	0.36	2.51E-04	1.92E-04	1.92E-06
10	0.60	1.00E-04	32.08	0.53	3.77E-04	2.87E-04	2.87E-06
11	0.80	1.33E-04	42.77	0.71	5.03E-04	3.83E-04	3.83E-06
12	0.10	1.67E-05	5.35	0.09	6.29E-05	4.79E-05	4.79E-07
13	0.60	1.00E-04	32.08	0.53	3.77E-04	2.87E-04	2.87E-06
14	1.00	1.67E-04	53.46	0.89	6.29E-04	4.79E-04	4.79E-06
15	2.00	3.33E-04	106.92	1.78	1.26E-03	9.58E-04	9.58E-06
16	2.20	3.67E-04	117.61	1.96	1.38E-03	1.05E-03	1.05E-05
17	1.50	2.50E-04	80.19	1.34	9.43E-04	7.19E-04	7.19E-06
18	2.00	3.33E-04	106.92	1.78	1.26E-03	9.58E-04	9.58E-06
19	2.50	4.17E-04	133.65	2.23	1.57E-03	1.20E-03	1.20E-05
20	4.20	7.00E-04	224.53	3.74	2.64E-03	2.01E-03	2.01E-05
21	6.50	1.08E-03	347.49	5.79	4.09E-03	3.11E-03	3.11E-05
22	6.50	1.08E-03	347.49	5.79	4.09E-03	3.11E-03	3.11E-05
23	4.00	6.67E-04	213.84	3.56	2.51E-03	1.92E-03	1.92E-05
24	1.50	2.50E-04	80.19	1.34	9.43E-04	7.19E-04	7.19E-06
25	12.50	2.08E-03	668.25	11.14	7.86E-03	5.99E-03	5.99E-05
26	11.50	1.92E-03	614.79	10.25	7.23E-03	5.51E-03	5.51E-05
27	3.00	5.00E-04	160.38	2.67	1.89E-03	1.44E-03	1.44E-05
28	3.50	5.83E-04	187.11	3.12	2.20E-03	1.68E-03	1.68E-05
29	1.50	2.50E-04	80.19	1.34	9.43E-04	7.19E-04	7.19E-06
30	2.00	3.33E-04	106.92	1.78	1.26E-03	9.58E-04	9.58E-06
31	9.50	1.58E-03	507.87	8.46	5.97E-03	4.55E-03	4.55E-05
32	1.05	1.75E-04	56.13	0.94	6.60E-04	5.03E-04	5.03E-06
33	0.75	1.25E-04	40.10	0.67	4.72E-04	3.59E-04	3.59E-06
Maximum	12.50	2.08E-03	668.25	11.14	7.86E-03	5.99E-03	5.99E-05
Minimum	0.10	1.67E-05	5.35	0.09	6.29E-05	4.79E-05	4.79E-07
Geometric mean	1.55	2.58E-04	82.80	1.38	9.74E-04	7.42E-04	7.42E-06
Average	2.68	4.46E-04	143.21	2.39	1.68E-03	1.28E-03	1.28E-05

Electrical resistivity and permeability tests

As mentioned above, electrical resistivity and permeability tests were applied combined at the four selected points. During the permeability tests, the data obtained such as infiltration rate, inflow volume and hydraulic conductivity were influenced by both permeabilities of the subsoil the primary and the secondary, the latter was mainly due to the network of small cracks observed at the surface.

Results at the infiltration point P1

Along with the permeability test applied at this point, located in the hanging wall of the fault, the ERT test was performed in profile B-B' (see Figure 2c). The results of this test showed a good contrast in the configuration of resistivities during the injection of water into the subsoil through the permeameter. Several observations can be highlighted from the results shown in Table 3, regarding the data generated by the permeameter, one of them is that the values of infiltration rate and hydraulic conductivity were decreasing as the tests progressed in time. This clearly indicates that the soil required more volume of water in the early stages of infiltration. There is not much information on this hydraulic response during the permeability tests, although a plausible explanation is that because the soil was dry, more water was required to moisten it. In other words, the pores of a portion of the soil were first saturated, through which the infiltrated water then began to circulate. According to the data shown by Freeze and Cherry, (1979), the hydraulic conductivity obtained from the local tests is numerically similar to that of sandy silt.

The results of the five ERT profiles, associated with the infiltration point P1 are depicted in Figure 9, which reveals a sequential reduction of the resistivity values in an area below the infiltration point. This reduction is associated with the ingress of water through the permeameter. It is observed that in a particular area, close to the infiltration point and shown in the magnified images of the boxes on the right, the resistivity values start between 50 and 100 Ω·m, with areas of 100 Ω·m predominating, but these values gradually decreased to magnitudes lesser than 50 Ω·m, observed in the last profile. The shape in which the zones with blue tones vary in that zone suggests a water flow as the main cause. This flow starts at the infiltration point at the surface and encompasses areas close to the fault plane. We can

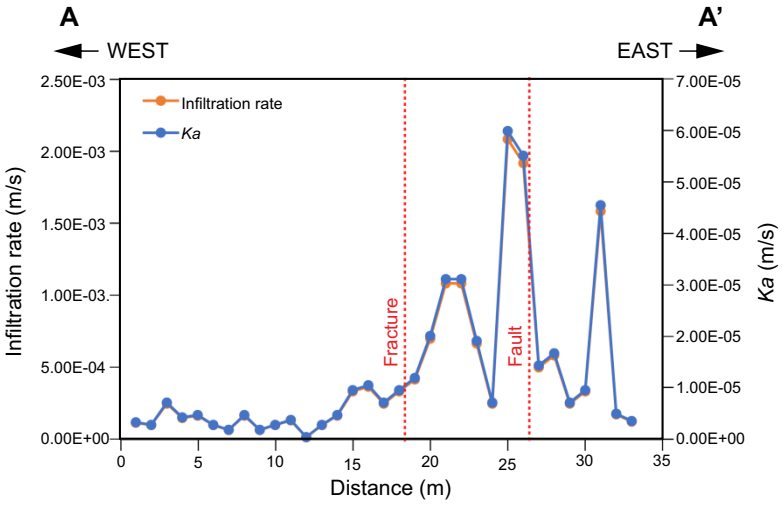

Figure 7. Variation profile of both the infiltration rate and the hydraulic conductivity (*Ka*), obtained from the tests with the Pask-type permeameter. As can be seen, both parameters maintain an approximate linear variation.

assume in this case that the fault zone is directly influencing the flow path since the infiltrated water tends to move towards the fault plane. All these changes occur at a depth no deeper than two meters.

As shown in Figure 9, there is also a zone of very low resistivity (less than 25 Ω·m) that is located in a zone deeper than two meters and that can be associated with the fault plane, probably due to retained moisture near the fault. It can be noted that this low-resistivity zone (strong blue color) increased as more water entered through the permeameter, in fact, this area was larger in the last profile, this is, in the latest permeability test.

Results at the infiltration point P2

Tests in point P2 were performed near the fracture (Figure 2c). Table 4 shows the results of the permeability test, where it is observed that the hydraulic parameters were reduced as the infiltration progressed, a response similar to that of point P1. However, at this point P2, the difference of parameters between tests 1 and 4 is much larger than in the case of point P1. In fact, the results of tests 1 and 2 contrast with those for tests 3 and 4, where an error in the experimental procedure would be more likely to explain this difference.

Figure 10 shows the results of the ERT tests. Unlike point P1, the variation of the resistivity suggests that at this point the water infiltrates more vertically, possibly influenced by the geometry of the fault plane. Changes in the resistivity through the four profiles occur mainly at a depth not greater than one meter and persist at values lesser than 75 Ω·m. It is observed that two zones of blue tones, corresponding to resistivities between 50–75 and 75–100 Ω·m, increase their area as more water infiltrates, in fact, the zone in light-blue color (75–100 Ω·m) deepens in more than 1.5 m.

Results at the infiltration point P3

The discontinuity associated with the infiltration point P3 corresponded to the fault. This point is located on the footwall block and the ERT profile covered partially the line A-A'. As observed in Table 5, the hydraulic parameters derived from the permeability test are in similar order of magnitude to those of point P1, and with decreasing variation of values of these parameters, similar to both points P1 y P2. Although, at this particular point P3 the difference between tests 1 and 4 is numerically not considerable.

Figure 11 shows perceptible changes in the resistivity configuration under the infiltration point, although, unlike the points P1 and P2, these changes associated with the infiltration process are larger in magnitude in the order of 150 to 225 Ω·m mainly. Before the infiltration process, the area below the infiltration point presented values between 200 and 225 Ω·m. However, as water entered the subsoil through the permeameter, this magnitude decreased to a range of 150 to 175 Ω·m. In particular, the light-yellow color zone, with a range of 175 to 200 Ω·m increases its area. In this case, there is no clear influence of the discontinuity plane during the filtering process, at least during the application of the ERT tests. However, a plausible explanation for the decrease in resistivity below the infiltration point is that the infiltrated water has dispersed throughout this zone of the subsoil, possibly influenced by the mechanical activity of the fault.

Results at the infiltration point P4

Infiltration point P4 is located near the fracture and Table 6 shows the results of the permeability tests at this point. Again, test 1 performed in this point presents the largest magnitudes of the hydraulic parameters. However, unlike the other experimental points, test 4 does

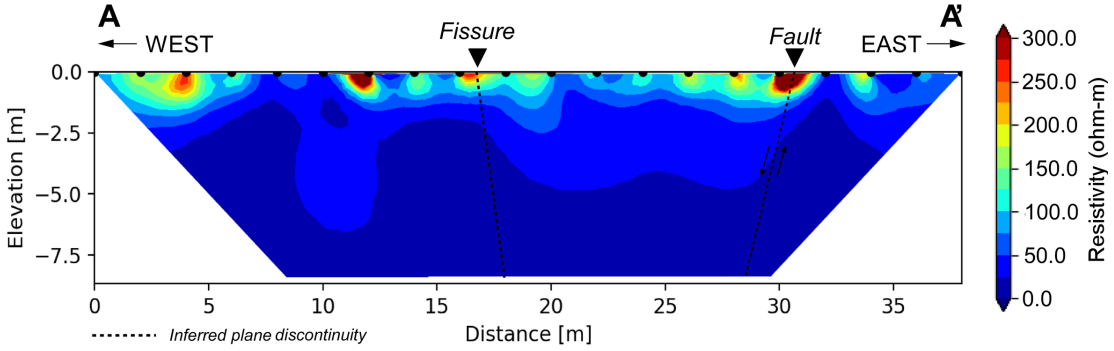

Figure 8. General ERT profile of the study area, which includes both discontinuities observed in the study area.

Table 3. Data resulted from the four permeability tests for point P1.

Test	Infiltration rate		Q		K_{fs}	K_a	
	cm/min	cm/s	cm³/min	cm³/s	cm/s	cm/s	m/s
DRY	-	-	-	-	-	-	-
1	3.01	5.02E-04	240.37	4.01	2.83E-03	2.15E-03	2.15E-05
2	1.2	2.00E-04	95.76	1.60	1.13E-03	8.58E-04	8.58E-06
3	0.82	1.37E-04	65.44	1.09	7.70E-04	5.86E-04	5.86E-06
4	0.9	1.50E-04	63.84	1.06	7.51E-04	5.72E-04	5.72E-06

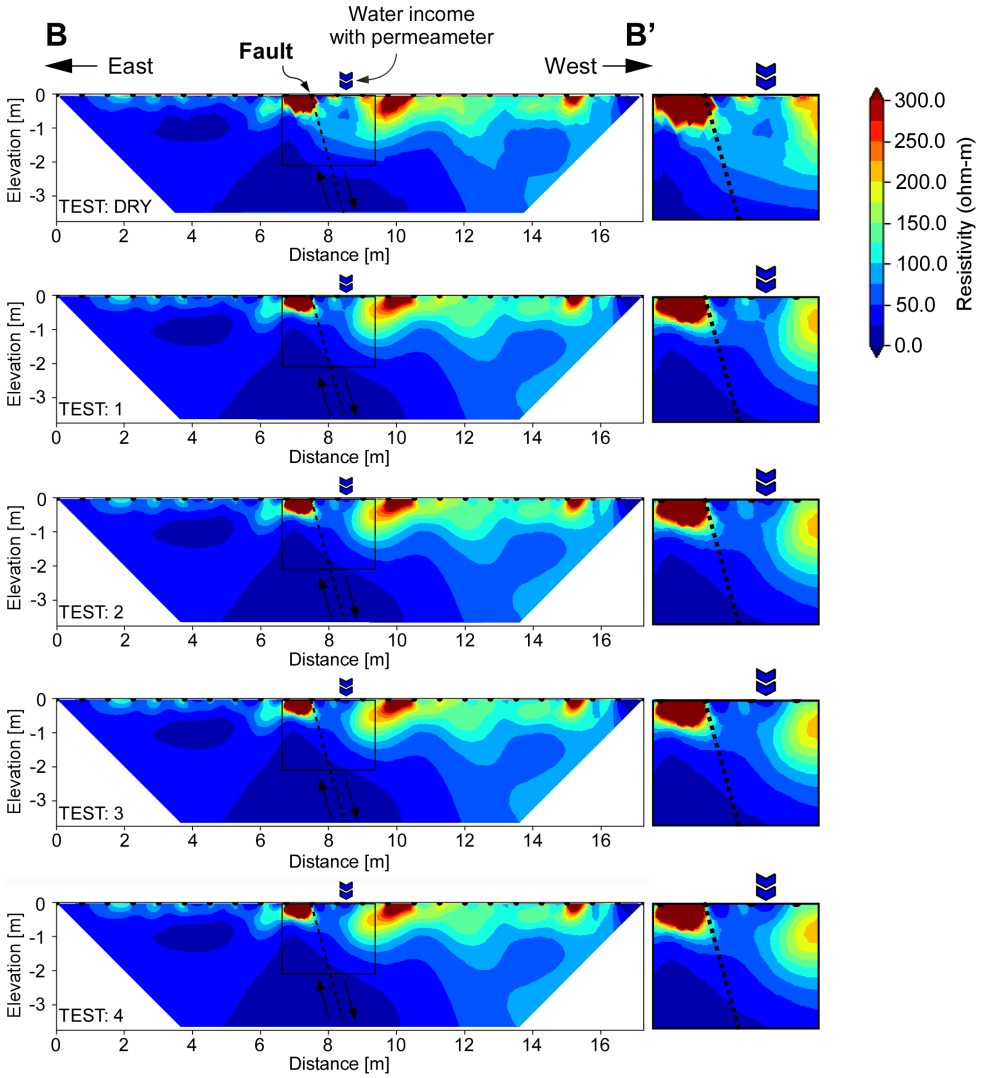

Figure 9. Results of the application of the five electrical resistivity tests in conjunction with that of permeability at the infiltration point P1. Unlike the other test points, in this particular point, the ERT profile was applied starting from the east in line B'-B (Figure 2c).

not present the smallest magnitudes of the hydraulic parameters, for this particular case, the smallest magnitudes are presented in tests 2 and 3, as observed in Table 6. This can be due to some errors during the test, but also to the effect of discontinuities on the soil and its hydraulic properties, as they can cause small fractures in the soil and thus randomly increase and decrease these properties.

Figure 12 shows the results of the ERT tests at point P4. As can be seen, there are no significant changes in resistivity in the area below the infiltration point, nor is there a clear influence of the discontinuity zone on the results derived from the permeability test. It is observed, however, that the area below the infiltration point already has low resistivities, below 100 Ω·m, probably because this area already retained some moisture, this may contribute to the result of resistivities observed at that point.

DISCUSSION

Within the analysis of the results, Figure 13 shows the comparison of the hydraulic parameters of the permeability tests in the four infiltration points. There are several observations to be considered from this figure, for example, at the infiltration point P2, the first

Table 4. Data derived from the four permeability tests for the infiltration point P2.

Test	Infiltration rate		Q		K_{fs}	K_a	
	cm/min	cm/s	cm³/min	cm³/s	cm/s	cm/s	m/s
DRY	-	-	-	-	-	-	-
1	10.53	1.76E-03	840.02	14.00	9.88E-03	7.53E-03	7.53E-05
2	9.8	1.63E-03	782.06	13.03	9.20E-03	7.01E-03	7.01E-05
3	0.4	6.67E-05	31.92	0.53	3.75E-04	2.86E-04	2.86E-06
4	0.26	4.33E-05	63.84	1.06	7.51E-04	5.72E-04	5.72E-06

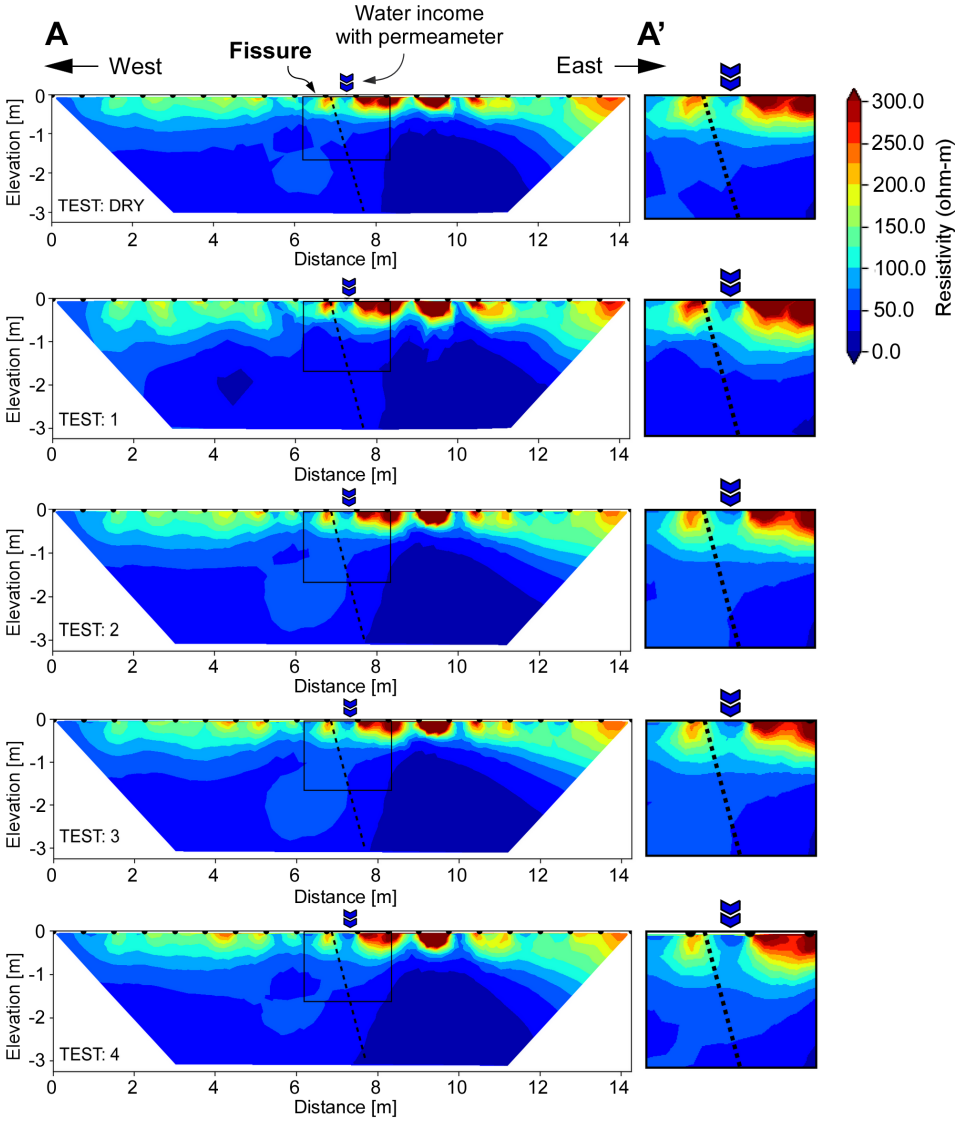

Figure 10. Results the application of the five ERT tests during the infiltration with the permeameter at the infiltration point P2. This sequence of profiles was partially applied in line A-A' of Figure 2c.

two tests present parameters significantly large compared to those of the last two tests. The results of the infiltration points P1 and P3 show a clear similarity in terms of the variation and magnitude of the parameters, while at infiltration point P4 the parameters were the lowest, perhaps that is why there are not considerably changes in the resistivity profiles of Figure 12.

On the other hand, the analysis of hydraulic properties of subsoils influenced by geological discontinuities has been a topic extensively studied (for example, Caine and Forster, 1999; Bense and Person, 2006; Bense, *et al.*, 2013; among others). It must be considered, however, that the conditions under which the hydraulic parameters are studied, particularly the conditions of the discontinuities, their geological environment and the scope and goal of the study are different for each particular case. For example, it is very common to find discontinuity analyses of regional scope for hydrocarbon studies, for which, understanding the hydraulic characteristics of both faults and fault zones is economically crucial for the oil industry. In hydrogeology studies, it is also important to understand the hydraulic characteristics

Table 5. Data derived from the four permeability tests for the infiltration point P3.

Test	Infiltration rate		Q		K_{fs}	K_a	
	cm/min	cm/s	cm³/min	cm³/s	cm/s	cm/s	m/s
DRY	-	-	-	-	-	-	-
1	3.96	6.60E-04	316.15	5.27	3.72E-03	2.83E-03	2.83E-05
2	1.6	2.67E-04	127.68	2.13	1.50E-03	1.14E-03	1.14E-05
3	1.34	2.23E-04	106.93	1.78	1.26E-03	9.58E-04	9.58E-06
4	1.24	2.07E-04	63.84	1.06	7.51E-04	5.72E-04	5.72E-06

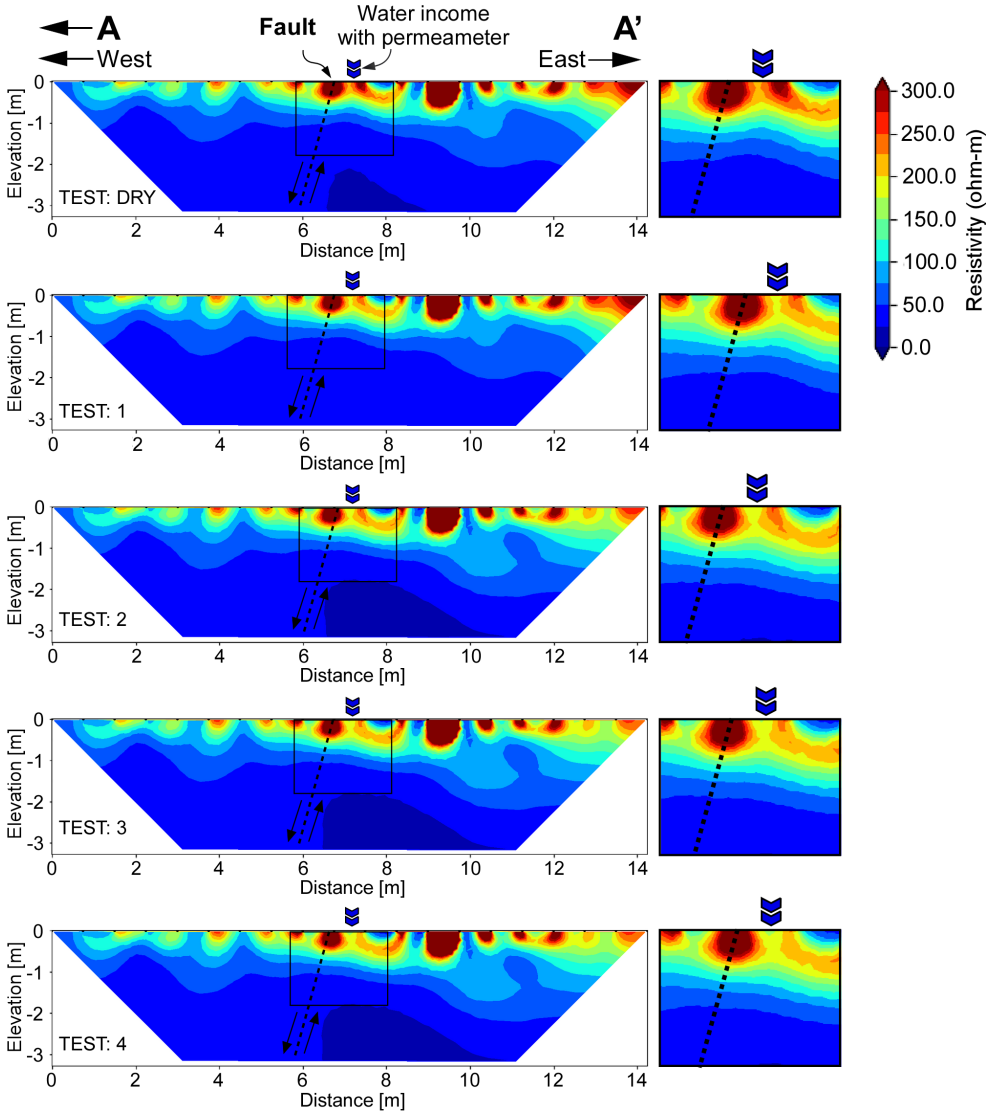

Figure 11. Results the application of the five ERT tests during the infiltration with the permeameter at the infiltration point P3. This sequence of profiles was partially applied in line A-A' of Figure 2c.

of discontinuities to enhance the extraction of water of better quality and in greater quantity, as already specified previously. It is also common to find that the analyzed discontinuities are regional with several kilometers long, even, the analyzed structures are inactive at the time of the research. In this regard, the degree of activity or inactivity is a factor that could have relevance in the hydraulic properties of the zone affected by a discontinuity, not only increasing its porosity and permeability (by causing small fractures during the mechanic activity of the discontinuity), but also reducing them, through processes such as the closure of flow paths in the porous network by rearrangement of clasts or cataclysms (Heynekamp *et al.*, 1999). In fact, the decrease in permeability can be more drastic when substances such as calcium carbonate are deposited by chemical precipitation on the spaces left during the rupture and rearrangement of sediments and rocks, or in small fractures associated with the main discontinuity. Figure 14 depicts filled fractures observed on an outcrop of the Oriente fault in the VA. Although this discontinuity is one of the most active in that valley, there are several points where the activity is negligible.

Table 6. Data derived from the four permeability tests for the infiltration point P4.

Test	Infiltration rate		Q		K_{fs}	K_a	
	cm/min	cm/s	cm³/min	cm³/s	cm/s	cm/s	m/s
DRY	-	-	-	-	-	-	-
1	1.04	1.73E-04	82.99	1.38	9.76E-04	7.44E-04	7.44E-06
2	0.28	4.67E-05	22.34	0.37	2.63E-04	2.00E-04	2.00E-06
3	0.28	4.67E-05	22.34	0.37	2.63E-04	2.00E-04	2.00E-06
4	0.36	6.00E-05	63.84	1.06	7.51E-04	5.72E-04	5.72E-06

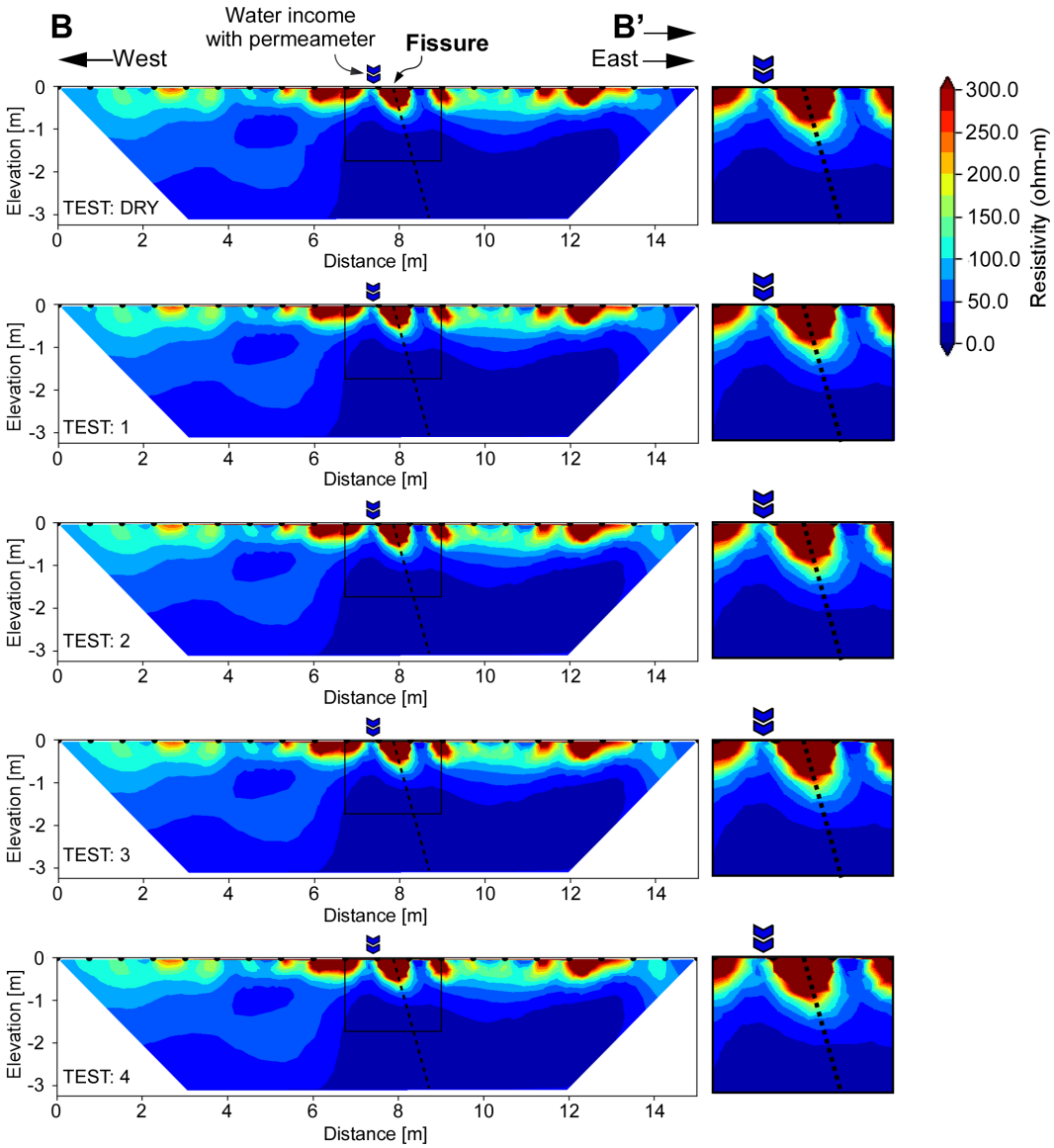

Figure 12. Results the application of the five electrical resistivity tests in conjunction with the permeameter infiltration at the infiltration point P4.

According to Pacheco-Martínez *et al.*, (2013), the time for these substances to be deposited in fractures in zones with the VA conditions is between 100 and 500 years, this particular point along the fault seemed to be accumulating strain. Over time, these filled cracks may rupture due to mechanical reactivation of the fault, or the filling substances may be diluted if any fluid interacts again with the medium. In these two cases the permeability of the fault could be affected again.

Among the various hydraulic parameters from areas adjacent to discontinuities, the permeability is highlighted, for this, Table 7 shows the results of hydraulic conductivities obtained for discontinuities that have remained inactive in the last 50 years. Some important characteristics are shown, mainly those that have a direct influence on the hydraulic conductivity, for example, whether the fault is reverse or normal. On this regard, notice that the reverse fault can be up to six times more permeable than those under extensional regime (1E-04

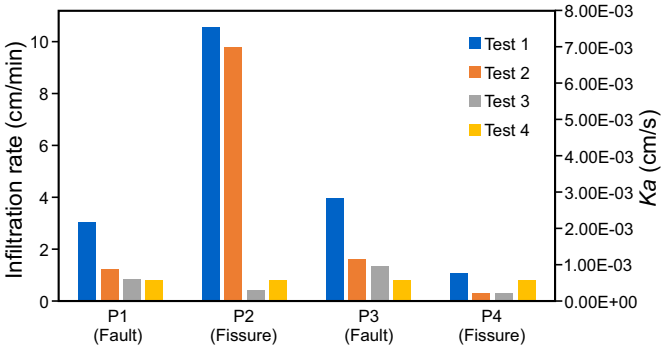

Figure 13. Comparison of the main hydraulic parameters obtained from the permeability tests for all infiltration points.

vs. 2.13E-10). It is also common to find that the hydraulic parameters obtained from the damaged zone and the core are higher than those measured in the zone not mechanically affected by the activity of the discontinuity. However, it should be noted that the intention of including this table is to show some case studies of hydraulic properties of faults in a general sense, not to compare and discuss some of their particular characteristics that affect the hydraulic response.

CONCLUSIONS

A targeted methodology was implemented to determine the hydraulic influence of two active discontinuities in the adjacent subsoil. A system of subsidence-related discontinuities formed by a fault and a fracture in the semi-arid Valley of Aguascalientes, were analyzed in their hydraulic parameters such as infiltration capacity and hydraulic conductivity. Currently, studies of the hydraulic properties of active faults and fractures are limited, which is the main global contribution and novelty of this work. The methodology included using a Pask-field permeameter, along with the Electrical Resistance Tomography (ERT) method. A profile of hydraulic parameters that covered both discontinuities was obtained, for this, 33 permeability tests were applied in a surface line perpendicular to both discontinuities, data were collected at one-meter intervals along a 33-meter profile. In addition, a general ERT profile of 38 meters long was performed, which also included both discontinuities in order to identify key structural and hydraulic characteristics. Later, in another series of tests, four fixed surface points close to the discontinuities (lesser than one meter away) were used to apply permeability tests and at the same time, ERT tests on 20-meter profiles were implemented. The purpose of these synchronous tests was to capture the path of the infiltrated water at the subsurface level using the ERT profiles and to visualize and quantify the potential influence of the two discontinuities on that process. The results demonstrated a strong hydraulic influence, as shown by the infiltration rates and hydraulic conductivities since the higher hydraulic values in the general profile resulted in points located between these two structures, being the two points with the highest values of infiltration rates of 2.08E-03 and 1.92E-03 m/s (12.5 and 11.5 cm/min) while the hydraulic conductivities for those two points resulted from 5.99E-05 and 5.51E-05 m/s. These two points are positioned to the west of the fault, while the lowest value of infiltration rate resulted in the order of 1.67E-05 m/s (0.1 cm/min) at a point to the west of the fracture, with a hydraulic conductivity of 4.79E-07 m/s. These numerical results showed a decrease in electrical resistivity during the successive application of permeability tests in which brackish water was injected into the soil. Except for point P4, which

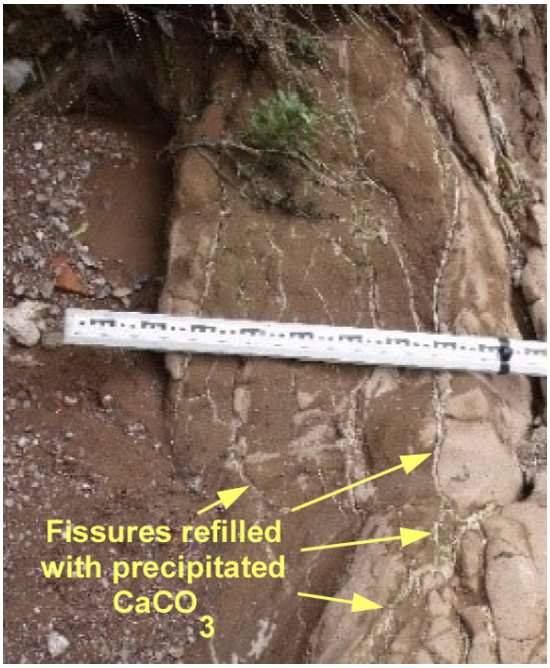

Figure 14. Photograph taken at an outcrop of the Oriente fault, Aguascalientes, where is observed how the fractures mechanically associated with the main structure were filled by calcium carbonate. The scale bar in the photograph shows approximately one meter.

is located at the west of the fracture, the resistivity values decreased as water infiltrated the subsoil through the permeameter, indicating a close relationship between water infiltration and electrical resistivity, showing the influence of the fault and fracture on subsurface water movement. This research contributes to a broader understanding of zones affected by discontinuities, particularly in the understanding of the hydraulic influence of local active fault systems, potentially contributing not only to local water resource management, but also to a regional understanding of subsurface water flow in faulted zones. Despite the results presented in this work, more investigation needs to be performed to, for instance, determine the path of the water at depth and where this water is finally stored, establish the variation of the quality of the water as it infiltrates through the discontinuity, etcetera.

Acknowledgments. Christian Emmanuel Rodríguez-Padilla is thankful for the financial support from CONAHCYT during his master studies.

Author contributions. M.H.M. and N.G.C. conceived the main idea and coordinated the overall investigation. They also integrated and organized all the information to write the paper manuscript. C.E.R.P. and L.G.M. performed the computations and coordinated the field experiments. J.P.M. verified the analytical methods and supervised the fieldwork. All authors discussed the results and revised the final manuscript.

Data avaliability statement. Data available on request from the authors. The data that support the findings of this study are available from the corresponding author upon reasonable request.

Declaration of Competing Interests. The authors declare that they have no known competing financial interests or personal relationships that could have appeared to influence the work reported in this article.

Funding. Funding was provided the Consejo Nacional de Ciencias, Humanidades y Tecnología (CONAHCyT) for the fellowship to support the Mater studies of C.E.R.P.

Table 7. Comparison of some characteristics of various discontinuities obtained in the literature, including the hydraulic conductivity.

Subsurface material affected by the discontinuity	Type of discontinuity	Activity in the last 50 years	Hydraulic conductivity of affected material (m/s)	Conditions of the study	Reference
Sandstones with variable porosity	Normal Fault	Inactive	~1E-04 to ~2E-07 (Converted from permeability, (mD))*	Measured into the host rock	(Antonellini and Aydin, 1994)
Unconsolidated sediments, sand and silt	Extensional Fault	Inactive	1.7E-04 to 8.9E-05	Measured in the fault core and the damage zone	(Bense *et al*., 2003)
High-porosity sandy sediments	Extensional fault	Inactive	~1E-04 to 1E-06 (Converted from permeability, (mD))*	Values of the mean for the fault zone	(Balsamo and Storti, 2010)
Granite, gneiss, and sedimentary rocks	Reverse fault	Inactive	1.1E-08 to 2.13E-10 (Converted from permeability, (m^2))*	Values of samples from the damaged zone at low confining pressures	(Evans *et al*., 1997)
Unconsolidated sediments, mainly sands	Extensional fault and fracture	Reactivated by subsidence	4.18E-07 to 5.22E-05	Measurements taken on surface close to discontinuities	This study

REFERENCES

Aguascalientes, Gobierno del Estado (2022). *Plan hídrico estatal 2021-2050 del estado de Aguascalientes*: Periódico oficial del estado de Aguascalientes edición extraordinaria, july 19 2022. Aguascalientes, Gobierno del estado de Aguascalientes, Instituto del Agua del Estado, 218 pp.

Antonellini, M., & Aydin, A. (1994). Effect of Faulting on Fluid Flow in Porous Sandstones: Petrophysical Properties1. *AAPG Bulletin*, *78*(3), 355–377. https://doi.org/10.1306/BDFF90AA-1718-11D7-8645000102C1865D

António, F., & Pacheco, L. (2002). Response to pumping of wells in sloping fault zone aquifers. Journal of Hydrology, 259(1), 116–135. https://doi.org/https://doi.org/10.1016/S0022-1694(01)00584-4

Aranda-Gómez, J. J., 1989, Geología preliminar del valle de Aguascalientes. *Revista Mexicana de Ciencias Geológicas*, *8*(1), 22–32.

Ball, L. B., Ge, S., Caine, J.S., Revil, A., & Jardani, A. (2010). Constraining fault-zone hydrogeology through integrated hydrological and geoelectrical analysis. *Hydrogeology Journal*, *18*(5), 1057–1067. https://doi.org/10.1007/s10040-010-0587-z

Balsamo, F., & Storti, F. (2010). Grain size and permeability evolution of soft-sediment extensional sub-seismic and seismic fault zones in high-porosity sediments from the Crotone basin, southern Apennines, Italy. *Marine and Petroleum Geology*, *27*(4), 822–837. https://doi.org/https://doi.org/10.1016/j.marpetgeo.2009.10.016

Bense, V. F., & Person, M. A. (2006). Faults as conduit-barrier systems to fluid flow in siliciclastic sedimentary aquifers. *Water Resources Research*, *42*(5), 1-18 https://doi.org/https://doi.org/10.1029/2005WR004480

Bense, V. F., Van den Berg, E. H., & Van Balen, R. T. (2003). Deformation mechanisms and hydraulic properties of fault zones in unconsolidated sediments; the Roer Valley Rift System, The Netherlands. *Hydrogeology Journal*, *11*(3), 319–332. https://doi.org/10.1007/s10040-003-0262-8

Bense, V. F., Person, M. A., Chaudhary, K., You, Y., Cremer, N., & Simon, S. (2008). Thermal anomalies indicate preferential flow along faults in unconsolidated sedimentary aquifers. *Geophysical Research Letters*, *35*(24), 1–6. https://doi.org/https://doi.org/10.1029/2008GL036017

Bense, V. F., Gleeson, T., Loveless, S. E., Bour, O., & Scibek, J. (2013). Fault zone hydrogeology. *Earth-Science Reviews*, *127*, 171–192. https://doi.org/https://doi.org/10.1016/j.earscirev.2013.09.008

Bredehoeft, J. D., Belitz, K., & Sharp-Hansen, S. (1992). The hydrodynamics of the Big Horn Basin: a study of the role of faults. *American Association of Petroleoum Geologists Bulletin*, *76*, 530–546.

Caine, J. S., & Forster, C. B. (1999). Fault zone architecture and fluid flow: Insights from field data and numerical modeling, in Haneberg, W.C., Mozley, P.S., Moore, J.C., and Goodwin, L.B., eds., Faults and subsurface fluid flow in the shallow crust. *American Geophysical Union Geophysical Monograph, 113*, 101–127.

Caine, J. S., & Tomusiak, S. R. A. (2003). Brittle structures and their role in controlling porosity and permeability in a complex Precambrian crystalline-rock aquifer system in the Colorado Rocky Mountain front range. *Geological Society of America Bulletin*, *115*(11), 1410–1424. https://doi.org/10.1130/B25088.1

Caine, J. S., Evans, J. P., & Forster, C. B. (1996). Fault zone architecture and permeability structure. *Geology*, *24*(11), 1025. https://doi.org/10.1130/0091-7613(1996)024<1025:FZAAPS>2.3.CO;2

Cilona, A., Aydin, A., & Johnson, N.M. (2015). Permeability of a fault zone crosscutting a sequence of sandstones and shales and its influence on hydraulic head distribution in the Chatsworth Formation, California, USA. *Hydrogeology Journal*, *23*(2), 405–419. https://doi.org/10.1007/s10040-014-1206-1

Constantin, J., Peyaud, J., Vergely, P., Pagel, M., & Cabrera, J. (2004). Evolution of the structural fault permeability in argillaceous rocks in a polyphased tectonic context. *Physics and Chemistry of the Earth, Parts A/B/C*, *29*(1), 25–41. https://doi.org/10.1016/j.pce.2003.11.001

Constantz, J., Herkelrath, W. N., & Murphy, F., (1988). Air Encapsulation During Infiltration. *Soil Science Society of America Journal*, *52*(1), 10–16. https://doi.org/https://doi.org/10.2136/sssaj1988.03615995005200010002x

Fronzi, D., Mirabella, F., Cardellini, C., Caliro, S., Palpacelli, S., Cambi, C., Valigi, D., & Tazioli, A., (2021). The Role of Faults in Groundwater Circulation before and after Seismic Events: Insights from Tracers, Water Isotopes and Geochemistry. *Water*, *13*(11), 1–21.

Dynamic Monitors (2022). *User Guide. ETC Pask (Constant Head well) permeameter for In-situ measurement of soil field saturated hydraulic conductivity*. Engineering Technologies Canada Ltd & Dynamic monitors, 1–31.

Elrick, D. E., & Reynolds, W. D. (1986). An analysis of the percolation test based in three-dimensional saturated-unsaturated flow from a cylindrical test hole. *Soil Science*, *142*(5). https://journals.lww.com/soilsci/fulltext/1986/11000/an_analysis_of_the_percolation_test_based_on.9.aspx

Evans, J. P., Forster, C. B., & Goddard, J. V., (1997). Permeability of fault-related rocks, and implications for hydraulic structure of fault zones. *Journal of Structural Geology*, *19*(11), 1393–1404. https://doi.org/10.1016/S0191-8141(97)00057-6

Freeze, A. R., & Cherry, J. A. (1979). *Groundwater*. Prentice Hall Inc.

Gannon, J. P., Burbey, T. J., Bodnar, R. J., & Aylor, J. (2012). Geophysical and geochemical characterization of the groundwater system and the role of Chatham Fault in groundwater movement at the Coles Hill uranium deposit, Virginia, USA. *Hydrogeology Journal*, *20*(1), 45–60. https://doi.org/10.1007/s10040-011-0798-y

González-Cervantes, N., Aranda-Gómez, J. J., Carranza-Castañeda, O., & Ortega-Obregón, C. (2019). Edad y origen de la paleocuenca continental de Teocaltiche, México. *Revista Mexicana de Ciencias Geológicas*, *36*(3), 393–410. https://doi.org/10.22201/cgeo.20072902e.2019.3.1391

Helena, P., Houben, G., & Himmelsbach, T. (2016). Numerical modeling of fracking fluid migration through fault zones and fractures in the North

German Basin. *Hydrogeology Journal*, *24*. https://doi.org/10.1007/s10040-016-1418-7

Hernández-Marín, M., González-Cervantes, N., Pacheco-Martínez, J., & Frías-Guzmán, D. H. (2015). Discussion on the origin of surface failures in the Valley of Aguascalientes, México. *Proceedings of the International Association of Hydrological Sciences*, *372*. https://doi.org/10.5194/piahs-372-235-2015.

Hernández-Marín, M., Pacheco-Martínez, J., Burbey, T. J., Carreón-Freyre, D. C., Ochoa-González, G. H., Campos-Moreno, G. E., & de Lira-Gómez, P. (2017). Evaluation of subsurface infiltration and displacement in a subsidence-reactivated normal fault in the Aguascalientes Valley, Mexico. *Environmental Earth Sciences*, 76(24), 1–12. https://doi.org/10.1007/s12665-017-7163-y.

Hernández-Marín, M.; Guerrero-Martínez, L.; Zermeño-Villalobos, A.; Rodríguez-González, L.; Burbey, T. J.; Pacheco-Martínez, J.; Martínez-Martínez, S. I.; & González-Cervantes, N. (2018). Spatial and Temporal Variation of Natural Recharge in the Semi-Arid Valley of Aguascalientes, Mexico. *Hydrogeology Journal*, *26*, 2811–2826. https://doi.org/10.1007/s10040-018-1819-x.

Heynekamp, M. R., Goodwin, L. B., Mozley, P. S., & Haneberg, W. C. (1999), Controls on fault zone architecture in poorly lithified sediments, Rio Grande Rift, New Mexico: implications for fault-zone permeability and fluid flow. In W. C., Haneberg, P. S., Mozley, J., Casey Moore, & L. B. Goodwin (Eds.), Faults and Subsurface Fluid Flow in the Shallow Crust. *AGU Geophysical Monograph*, *113*, 27–51.

Lee, C. F., Zhang, J. M., & Zhang, Y. X. (1993). Evolution and origin of the ground fissures in Xian, China. *Engineering Geology*, *43*(1), 45–55.

Loza-Aguirre, I., Nieto-Samaniego, A. F., Alaniz-Alvarez, S. A., & Iriondo, A. (2008). Relaciones estratigráfico-estructurales en la intersección del sistema de fallas San Luis-Tepehuanes y el graben de Aguascalientes, México Central: *Revista Mexicana de Ciencias Geológicas*, *25*(3), 533-548.

Martin, R. V, Van Arsdale, R. B., & Harrison, V. J. (2023). Possible Fault Communication between the Memphis Sand Aquifer and the Mississippi River. *Environmental & Engineering Geoscience*, *29*(2), 105–114. https://doi.org/10.2113/EEG-D-22-00050

Nieto-Samaniego, A. F., Alaniz-Álvarez, S. A., & Camprubí, A. (2005). Mesa Central of México: Stratigraphy, structure, and Cenozoic tectonic evolution. *Boletín de la Sociedad Geológica Mexicana*. *57*(3), 285-318.

Nieto-Samaniego, A. F., Del Pilar-Martínez, A., Suárez-Arias, A. M., Angeles-Moreno, E., Alaniz-Álvarez, S. A., Levresse, G., Xu, S., Olmos-Moya, M. J. P., & Báez-López J. A. (2023). Una revisión de la geología y evolución tectónica cenozoicas de la Mesa Central de México. *Revista Mexicana de Ciencias Geológicas*, *40*(2), 187-213. https://doi.org/10.22201/cgeo.20072902e.2023.2.1736.

Ochoa-González, G. H., Carreón-Freyre, D., Cerca, M., & López-Martínez, M (2015). Assessment of groundwater flow in volcanic faulted areas. A study case in Queretaro, Mexico. *Geofísica Internacional*, *54*(3). https://doi.org/10.1016/j.gi.2015.04.016

Pacheco-Martínez, J., Hernandez-Marín, M., Burbey, T. J., González-Cervantes, N., Ortíz-Lozano, J. T., Zermeño-De-Leon, M. E., & Solís-Pinto, A. (2013). Land subsidence and ground failure associated to groundwater exploitation in the Aguascalientes Valley, México. *Engineering Geology*, *164*. https://doi.org/10.1016/j.enggeo.2013.06.015

Petrie, E. S., Petrie, R. A., & Evans, J. P. (2014). Identification of reactivation and increased permeability associated with a fault damage zone using a multidisciplinary approach. *Journal of Structural Geology*, *59*, 37–49. https://doi.org/https://doi.org/10.1016/j.jsg.2013.11.008

Reyes-Cedeño, I. G., Hernández-Marín, M., Pacheco-Guerrero, A. I., & Gannon, J. P. (2023). Application of Vertical Electrical Sounding and Toxicity Tests for the Analysis of Vertical Hydraulic Connectivity through the Vadose Zone. *Water*, *16*(2), 1–20.

Reynolds, W. D. (1993). Saturated hydraulic conductivity: field measurement. En Carter M.R. (Ed.), *Soil Sampling and Methods of Analysis* (pp. 599–613).

Rugh, D. F., & Burbey, T. J., (2008), Using saline tracers to evaluate preferential recharge in fractured rocks, Floyd County, Virginia, USA. *Hydrogeology Journal*, *16*(2), 251–262. https://doi.org/10.1007/s10040-007-0236-3

Seaton, W. J., & Burbey, T. J. (2005) Influence of ancient thrust faults on the hydrogeology of the blue ridge province. *Groundwater*, *43*(3), 301–313. https://doi.org/https://doi.org/10.1111/j.1745-6584.2005.0026.x

Servicio Geológico Mexicano (1998). Carta geológico-minera Aguascalientes F13-9. *Servicio Geológico Mexicano*, 1 map.

Stoessell, R. K., & Prochaska, L. (2005). Chemical Evidence for Migration of Deep Formation Fluids into Shallow Aquifers in South Louisiana. *Gulf Coast Association of Geological Societies Transactions*, *55*, 794–808.

Streeter, V., & Wylie, E. B., (1975), *Fluid Mechanics* (6ta ed.). McGraw Hill.